Non-Markovian effects in time-resolved fluorescence spectrum of molecular aggregates: Tracing polaron formation

Andrius Gelzinis,[1,2] Darius Abramavicius,[1,3] and Leonas Valkunas[1,2,*]

[1]*Department of Theoretical Physics, Faculty of Physics of Vilnius University, Sauletekio Avenue 9, Build. 3, LT-10222 Vilnius, Lithuania*

[2]*Center for Physical Sciences and Technology, Savanoriu Avenue 231, LT-02300 Vilnius, Lithuania*

[3]*State Key Laboratory of Supramolecular Complexes, Jilin University, 2699 Qianjin Street, Changchun 130012, PR China*

(Received 6 September 2011; published 15 December 2011)

Time-resolved fluorescence spectroscopy of molecular aggregates is described using the response function theory, which incorporates exciton dynamics through nonequilibrium Green's functions. The dynamics are simulated using nonperturbative density matrix theory, which allows us to describe spectral and temporal signatures of various system-bath coupling regimes. We find that the conventional excitonic picture of eigenstates is valid in the Markovian regime. In the non-Markovian regime, the exciton concept breaks down and renormalized quantities can be introduced. Effective intermolecular coupling, widely used in polaron theories, can be used to account for the effects of the bath.

DOI: 10.1103/PhysRevB.84.245430 PACS number(s): 78.47.J−, 71.35.Aa, 71.38.−k

I. INTRODUCTION

Electronic excitation dynamics in molecular aggregates is extensively studied both theoretically[1,2] and experimentally.[3–7] Recent development of two-dimensional (2D) electronic spectroscopy has led to a greater understanding about the exciton relaxation and dephasing in these systems.[8] Even though simulations of excitonic aggregates of various sizes are possible,[9–12] interpretation of the results is a considerable challenge, and the very applicability of the exciton approach when subjected to the coupling to different types of the bath ranging from water to proteins is still under debate.[7] The conventional Redfield theory, which is the second order to the system-bath coupling,[2] has been successful for both small[13,14] and large[11] systems, but a range of invoked assumptions are not easy to validate for large aggregates. The strong system-bath interaction limit is problematic for these perturbative approaches, although it was recently shown that perturbative treatment of intermolecular couplings instead of system-bath coupling is possible.[15] The electronic states in molecular solids are known to be strongly affected by phonons: these can transform the states themselves. The problem of electron-in-the-lattice has been extensively studied using the Holstein Hamiltonian,[16–20] which was shown to yield useful results for photosynthetic systems as well.[21–23] The net effect is that the lattice experiences deformation, which leads to localization and trapping of delocalized electronic states. The system then can be described by effective parameters such as effective mass, effective coupling, and effective bandwidth.[24]

Absorption and fluorescence (emission) spectroscopy are the core experimental tools when probing electronic states in molecular aggregates. They can be denoted as conjugate techniques since the absorption probes the electronic ground-state equilibrium (of the bath), while the fluorescence probes the electronic excited-state equilibrium. Time-resolved fluorescence (TRF) adds an additional degree of freedom. It is a probe of the excited-state relaxation dynamics in molecular systems[25,26] *after excitation by laser pulses*. It was recently demonstrated that TRF is useful for studying disordered systems.[27] The TRF has a lot of advantages compared to other types of time-resolved spectroscopies such as pump probe or the recently developed 2D coherent spectroscopy, as the TRF spectra are much easier to analyze due to absence of the excited-state absorption and the ground-state bleaching processes (and also much more computationally friendly since double excitons are not involved). Thus, the TRF can be considered as the direct probe of the excited-state relaxation dynamics.[28]

Theoretical description of the TRF can be based on the third-order response function theory[25,29] and involves the system relaxation dynamics due to the coupling with the bath. For a single molecule using the adiabatic approximation for electronic energy levels and the Gaussian bath, exact expressions for the third-order response function can be obtained using lineshape functions[29] (the second-order cumulants) and TRF can be easily calculated (shown in the following). The TRF spectra of a two-level electronic system then demonstrates how the spectral lineshapes turn from Lorentzian to Gaussian and how the Stokes shift emerges (Fig. 1). As is well known, in that case, the regimes corresponding to fast- and slow-bath dynamics can be clearly identified for an overdamped Brownian oscillator bath spectral density by inspecting the dimensionless parameter $2\lambda k_B T \gamma^{-2}$, where λ is the system-bath coupling strength, $k_B T$ is the thermal energy, and γ^{-1} is the relaxation time scale of bath fluctuations.[29] However, this theory may be violated for molecular aggregates as the exciton levels may cross each other due to fluctuations.

The same issues are inherent in the Redfield theory when applied to aggregates. It is suitable for exciton transfer in the case of weak system-bath interaction and when the bath dynamics are relatively fast.[7,30–33] Recently, the Redfield equation was challenged as unsuitable for energy-transfer analysis in photosynthetic systems.[33] The full Redfield theory is sometimes plagued by the positivity problem as it can not guarantee non-negative population values.[34] To overcome this problem, the secular approximation is often employed,[30] but it leads to the stationary solution corresponding to the Boltzmann distribution of the *bare* system. Various second-order quantum master equations (QMEs) were studied recently,[35] and it was demonstrated that nonsecular theories lead to deviations from excitonic Boltzmann distribution, as is the case of the

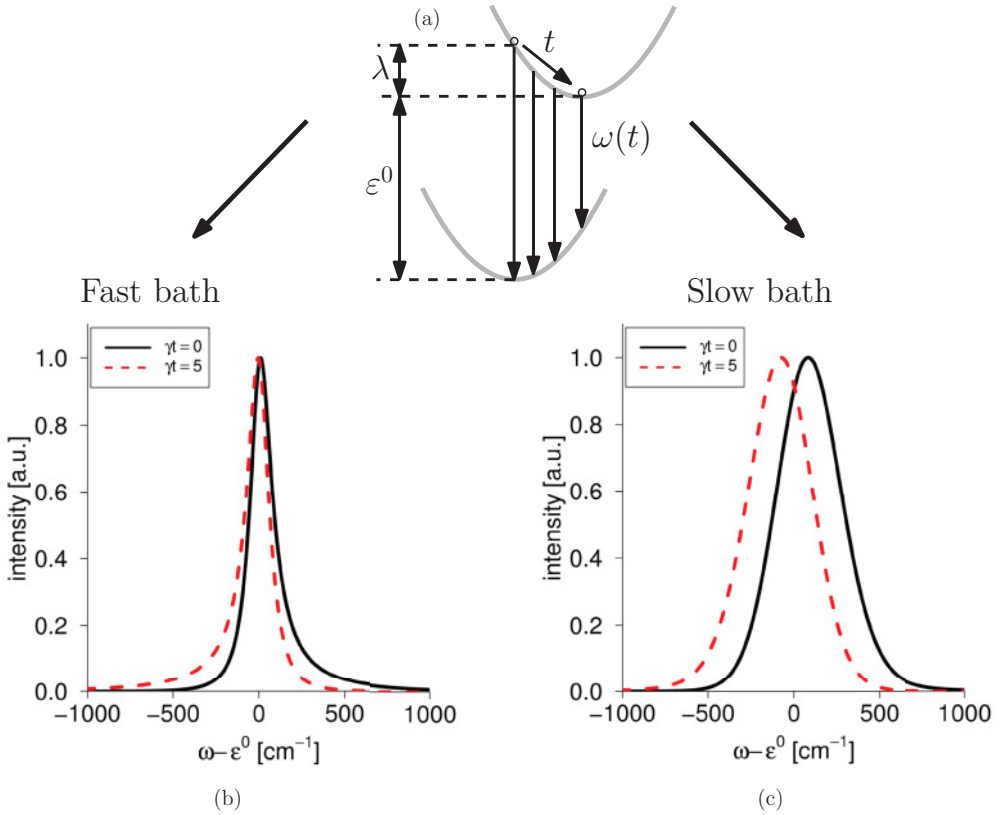

FIG. 1. (Color online) (a) Schematic representation of a TRF in a two-level molecule (for definition of parameters, see the text), (b) the TRF spectra in the fast-dynamics (Markovian) regime ($2\lambda k_B T\gamma^{-2} = 0.1479$), and (c) the slow-dynamics regime ($2\lambda k_B T\gamma^{-2} = 14.79$). In both cases, the bath spectral density corresponds to the overdamped Brownian oscillator and the reorganization energy $\lambda = 100$ cm^{-1} is chosen for calculations (see Sec. II).

fourth-order QME.[36] In order to learn more realistic equilibrium solutions, the nonperturbative theory is needed.

A possible strategy to overcome these inconsistencies of approximate methods is to study small aggregates using nonperturbative theory and to extend the obtained insights and conclusions to large aggregates. Various approaches, such as path integral formalism or direct integration of the Nakajima-Zwangzig equation, could be used in order to determine the system evolution nonperturbatively.[37] Hierarchical equations of motion (HEOM), which follow from another nonperturbative theory of open quantum system dynamics for a reduced density matrix,[38,39] gained a lot of attention by their recent application to electronic excitation dynamics.[40] The HEOM theory was used to analyze dynamics in a separate peripheral light-harvesting LH2 complex (the B850 ring) of photosynthetic bacteria and between them.[41] The HEOM theory was used to model the spectroscopic experiments as well: time-dependent emission[40] and absorption spectra[42] of molecular systems were calculated. Also, the 2D spectra of a molecular dimer[43] and the Fenna-Matthews-Olson (FMO) protein complex[44] were simulated. As a nonperturbative theory, the full HEOM theory is numerically very expensive and scales unfavorably with the system size. Some approximate versions, appropriate for relatively high temperatures, were developed.[45,46] They approximate the correlation function by a finite set of exponential decays. In this work, we use the HEOM theory to describe the TRF of a molecular aggregate.

It was demonstrated using the HEOM theory that equilibrium excitonic populations in the B850 ring do not fully coincide with excitonic Boltzmann distribution.[41] Thus, it is clear that the bath affects the equilibrium states of the system. Effects caused by the bath play a significant role in polaron theory, where effective coupling is often employed to demonstrate that strong system-bath coupling reduces the effective bandwidth of the electronic excitations in the system.[24,36] The exciton system is different from the electron-in-the-lattice system since excitons are nonequilibrium particles. The influence of the bath on the excitonic systems is still not perfectly clear, and the simplest excitonic description needs to be revisited. In this paper, we study exciton dynamics in the case of moderate and strong system-bath interaction and its manifestation in the TRF spectroscopy. We find that the excitonic picture is valid only in a specific range of system-bath parameters and it depends on the delay after excitation.

This paper is organized as follows. In Sec. II, we develop the microscopic theory of the TRF for molecular aggregates. First, we describe our model Hamiltonian. Second, we show how the third-order response theory is used to calculate the TRF spectra. Third, we present the HQME (an approximate HEOM theory used in this paper for calculations), and we describe how to connect the TRF with the HQME. Then, in Sec. III, we present the simulated time-resolved fluorescence spectra of a dimer. Special interest is paid to finding out how bath parameters affect the spectra. In Sec. IV, we discuss

the features of Markovian and non-Markovian regimes and their manifestations in the TRF spectra and then present calculations of evolutions of density matrix elements of the system under consideration. Then, we analyze how stationary states of the system are affected by the bath and introduce effective coupling as a qualitative parameter to account for the effects of the bath. Finally, the conclusions are given in Sec. V.

II. MICROSCOPIC THEORY OF TIME-RESOLVED FLUORESCENCE

A. Model Hamiltonian

We consider an aggregate made of N weakly interacting molecules (chromophores) embedded in some molecular environment (solvent, solid matrix, protein) as schematically shown in Fig. 2. The chromophores compose an open quantum system, which is coupled to the bath. The total Hamiltonian then consists of the following terms:

$$\hat{H} = \hat{H}_e + \hat{H}_{\text{ph}} + \hat{H}_{e\text{-ph}} + \hat{H}_{e\text{-}F}. \tag{1}$$

The chromophores are neutral and interact through dipole-dipole electrostatic fields. Additionally, electron exchange between molecules is neglected. The electronic (system) part $\hat{H}_e$ is then determined by the well-known Frenkel exciton Hamiltonian.[1] In the system we consider, only the ground state, where no excitation is present, and the single-exciton manifold, where one molecule is excited. Such blocks are described by

$$\hat{H}_e = \sum_n^N \left(\varepsilon_n^0 + \lambda_n\right)|n\rangle\langle n| + \sum_{m\neq n}^N J_{mn}|m\rangle\langle n|. \tag{2}$$

Here, $|n\rangle$ represents a state of the aggregate where only the nth molecule is in its excited electronic state and all others are in their ground state, ε_n^0 is the energy gap between the excited and ground states of the nth molecule, λ_n is the reorganization energy reflecting the excited-state potential displacement in comparison with that in the ground state of the nth molecule, and J_{mn} is the resonance coupling between the mth and nth molecules. The ground state is isolated and its energy is chosen to be 0. This setup allows us to introduce excitonic delocalized states of the electronic aggregate, i.e., the excitons. The number of possible excitons (single excitons) is N: they form a band of states of $\sim 2zJ$ width (J is the maximal value of the resonance coupling between the nearest-neighboring molecules, z is the molecular coordination number in the aggregate), separated from the ground state by an optical gap, which is of the order of a mean transition energy.

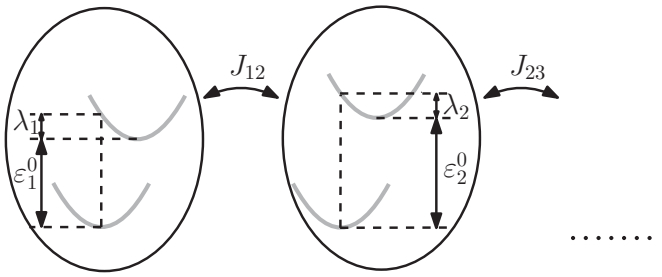

FIG. 2. Schematic representation of a molecular aggregate (see text for details).

The bath is modeled by an infinite set of harmonic oscillators

$$\hat{H}_{\text{ph}} = \sum_j \frac{\omega_j}{2}\left(\hat{p}_j^2 + \hat{x}_j^2\right), \tag{3}$$

which are linearly coupled to chromophores

$$\hat{H}_{e\text{-ph}} = -\sum_n^N \sum_j \omega_j d_{nj}\hat{x}_j|n\rangle\langle n|. \tag{4}$$

The bath parameters are as follows: ω_j, $\hat{p}_j$, and $\hat{x}_j$ are the frequency, momentum, and coordinate (both dimensionless) of the jth bath mode. d_{nj} is the dimensionless displacement of the equilibrium configuration of the jth bath mode between the ground and excited electronic states of the nth molecule. In this scheme, the reorganization energy $\lambda_n = \sum_j \omega_j d_{nj}^2/2$ is the main parameter characterizing the system-bath coupling. All parameters are indicated in Fig. 2. Note that we use frequency units for energy ($\hbar = 1$) throughout the paper. The system-bath coupling expression can be simplified by introducing distinct system and bath operators $\hat{Q}_n = |n\rangle\langle n|$ and $\hat{F}_n = -\sum_j \omega_j d_{nj}\hat{x}_j$:

$$\hat{H}_{e\text{-ph}} = \sum_n^N \hat{F}_n\hat{Q}_n. \tag{5}$$

Notice that this form denotes that the bath is not coupled to the electronic ground state.

It can be shown[30] that the effects of the bath are determined by a fluctuation correlation function

$$C_{mn}(t) = \text{Tr}_{\text{ph}}\left[\hat{F}_m^I(t)\hat{F}_n^I(0)\hat{\rho}_{\text{eq}}^{\text{ph}}\right]. \tag{6}$$

Here,

$$\hat{F}_m^I(t) = e^{i\hat{H}_{\text{ph}}t}\hat{F}_m e^{-i\hat{H}_{\text{ph}}t} \tag{7}$$

represents operator $\hat{F}_m$ in the interaction representation. The correlation function depends on temperature T of the bath. It is convenient to derive the temperature-independent bath characteristics, the spectral density, which is given by the Fourier transform of the imaginary part of the correlation function[29]

$$C''_{mn}(\omega) = i\int_{-\infty}^{\infty} e^{i\omega t}\text{Im}C_{mn}(t)dt. \tag{8}$$

The correlation function can be now conveniently expressed as

$$C_{mn}(t) = \frac{1}{\pi}\int_{-\infty}^{+\infty}\frac{1}{1-e^{-\beta\omega}}e^{-i\omega t}C''_{mn}(\omega)d\omega. \tag{9}$$

Here, $\beta = (k_B T)^{-1}$ and k_B is the Boltzmann constant. In the following, we assume that bath modes associated with different chromophores are not correlated:

$$C''_{mn}(\omega) = \delta_{mn}C''_n(\omega). \tag{10}$$

Using this formulation, we have the following independent spectral densities:

$$\mathcal{C}_n''(\omega) = \pi \sum_j \frac{\omega_j^2 d_{nj}^2}{2}[\delta(\omega-\omega_j) - \delta(\omega+\omega_j)]. \quad (11)$$

However, instead of infinite sum over delta sticks, we use a continuous function representing an overdamped Brownian oscillator, which has been widely used for describing the spectral properties of molecular aggregates:[7,8,10–12,14,33,40–44]

$$\mathcal{C}_n''(\omega) = 2\lambda_n \frac{\omega\gamma_n}{\omega^2+\gamma_n^2}; \quad (12)$$

γ_n^{-1} is the decay time of the bath correlation for the nth chromophore and λ_n (the reorganization energy) now describes the coupling strength.

The last term in the Hamiltonian represents coupling to a classical radiation field

$$\hat{H}_{e\text{-}F} = \hat{\boldsymbol{\mu}} \cdot \boldsymbol{\mathcal{E}}(t) \equiv \sum_n^N [\boldsymbol{\mu}_{gn} \cdot \boldsymbol{\mathcal{E}}(t)](|n\rangle\langle g| + |g\rangle\langle n|), \quad (13)$$

where $\hat{\boldsymbol{\mu}}$ is the dipole operator, $\boldsymbol{\mu}_{gn}$ is the transition dipole vector for molecule n, and $|g\rangle$ is the ground state of the aggregate when no excitations are present. In the following, we assume that the field is a short excitation pulse, much shorter than the relevant bath-induced system dynamics. It thus can select relevant resonant exciton states, but their evolution is much slower than the pulse duration. In this case, the incident field is responsible only for the preparation step for the later system evolution.

B. Time-resolved fluorescence of the aggregate

The equilibrium fluorescence (emission) is a process wherein a molecule relaxes from an excited state into its ground state by a photon emission. Such a process is described in the density matrix theory by two interactions with the radiation field (left and right sides) due to $\hat{H}_{e\text{-}F}$.[29] It is thus reverse to the linear response, which describes, e.g., absorption. However, the excited-state preparation process is not included in such a description of the emission. The TRF is the more general concept, which tracks the time after the excitation event. This delay time allows us to observe the relaxation process in the excited state. As described in the Introduction, the TRF is a probe of the excited-state relaxation dynamics. Possible experimental realizations with femtosecond resolution have been described elsewhere.[28] Using the density matrix theory, the excitation process involves two primary interactions with the radiation field, while two more are needed for the later emission, as described previously. The TRF is characterized by four system-field interaction events and thus falls into the third-order nonlinear response theory.

The third-order response function relates the induced third-order optical polarization $P^{(3)}(t)$ with the incoming electric field $E_{\text{in}}(t)$:

$$P^{(3)}(t) = \iiint dt_3\, dt_2\, dt_1\, R^{(3)}(t_3,t_2,t_1) E_{\text{in}}(t-t_3) \times E_{\text{in}}(t-t_3-t_2) E_{\text{in}}(t-t_3-t_2-t_1). \quad (14)$$

The outgoing signal field can then be calculated using the Maxwell equations. Here, for simplicity we assume that the output signal is proportional to the polarization: $E_{\text{out}}(t) \propto P^{(3)}$. The third-order response function $R^{(3)}(t_3,t_2,t_1)$ describes all nonlinear properties of the system up to the third order. Using the Liouville space notation [for density matrix we have $|\rho\rangle\rangle \Leftrightarrow \hat{\rho}$, and $\langle\langle\boldsymbol{\mu}|\rho\rangle\rangle \Leftrightarrow \mathrm{Tr}(\hat{\boldsymbol{\mu}}\hat{\rho})$], it can be given as the following trace:[29]

$$R^{(3)}(t_3,t_2,t_1) = \mathrm{i}^3 \langle\langle\boldsymbol{\mu}|\hat{\mathcal{G}}(t_3)\hat{\boldsymbol{\mu}}^l\hat{\mathcal{G}}(t_2)\hat{\boldsymbol{\mu}}^l\hat{\mathcal{G}}(t_1)\hat{\boldsymbol{\mu}}^l|\rho_{gg}\rangle\rangle, \quad (15)$$

where $|\rho_{gg}\rangle\rangle$ represents the initial ground state, $\hat{\mathcal{G}}$ is the free-field Liouville-space evolution superoperator, and $\hat{\boldsymbol{\mu}}^l$ is a dipole superoperator. The latter can be expressed as a sum of two terms that correspond to action from the left, $\hat{\boldsymbol{\mu}}_L^l$, and from the right, $\hat{\boldsymbol{\mu}}_R^l$:

$$\begin{aligned} \hat{\boldsymbol{\mu}}^l|\rho\rangle\rangle &= \hat{\boldsymbol{\mu}}_L^l|\rho\rangle\rangle + \hat{\boldsymbol{\mu}}_R^l|\rho\rangle\rangle, \\ \hat{\boldsymbol{\mu}}_L^l|\rho\rangle\rangle &\Leftrightarrow \hat{\boldsymbol{\mu}}\hat{\rho}, \\ \hat{\boldsymbol{\mu}}_R^l|\rho\rangle\rangle &\Leftrightarrow -\hat{\rho}\hat{\boldsymbol{\mu}}. \end{aligned} \quad (16)$$

The trace is taken over the whole system + bath composite supersystem. Expanding all commutators gives eight terms in the total response function, which may be associated with various processes. For the TRF calculations, we can make some restrictions. The first part of an incoming field is a single pulse, which resonantly excites a single exciton state e and creates its population. Time t_1 is thus limited within the excitation pulse and $\hat{\mathcal{G}}(t_1)$ is responsible for the preparation process. The second delay t_2 is the "gap" when the field is off. During the third delay time t_3, the emission takes place by a transition from some exciton state e' to the ground state and the dynamics of $e'g$ quantum coherence generates the outgoing field, which is being detected by a spectrograph [this outgoing field thus serves as $E_{\text{in}}(t-t_3)$ in Eq. (14)]. Within these restrictions, only two terms in the response function are related to the TRF (Refs. 25 and 29):

$$\begin{aligned} R_{\text{TRF}}(t_3,t_2,t_1) = \mathrm{i}^3\big[&\langle\langle\boldsymbol{\mu}|\hat{\mathcal{G}}(t_3)\hat{\boldsymbol{\mu}}_R^l\hat{\mathcal{G}}(t_2)\hat{\boldsymbol{\mu}}_L^l\hat{\mathcal{G}}(t_1)\hat{\boldsymbol{\mu}}_R^l|\rho_{gg}\rangle\rangle \\ &+ \langle\langle\boldsymbol{\mu}|\hat{\mathcal{G}}(t_3)\hat{\boldsymbol{\mu}}_R^l\hat{\mathcal{G}}(t_2)\hat{\boldsymbol{\mu}}_R^l\hat{\mathcal{G}}(t_1)\hat{\boldsymbol{\mu}}_L^l|\rho_{gg}\rangle\rangle\big]. \end{aligned} \quad (17)$$

We next assume the impulsive limit for the excitation and for detection and denote the free-field propagation time as $t \equiv t_2$. The TRF is then given as

$$F(\omega,t) = \mathrm{Re}\int_0^\infty d\tau\, e^{\mathrm{i}\omega\tau}\mathrm{i}R_{\text{TRF}}(\tau,t,t_1\to 0). \quad (18)$$

We have assumed that, during the excitation, only one excited-state population is resonantly excited. It can be achieved when the incoming field frequency is tuned to specific transition energy in the system and the spectrum of the pulses are not too broad, thus we set

$$\hat{\boldsymbol{\mu}}_R^l\hat{\mathcal{G}}(0)\hat{\boldsymbol{\mu}}_L^l|\rho_{gg}\rangle\rangle = \hat{\boldsymbol{\mu}}_L^l\hat{\mathcal{G}}(0)\hat{\boldsymbol{\mu}}_R^l|\rho_{gg}\rangle\rangle \approx -|\rho_{ee}^{(g)}\rangle\rangle, \quad (19)$$

where $|\rho_{ee}^{(g)}\rangle\rangle$ denotes the excited-state e population with the bath equilibrium corresponding to the ground state. Therefore, the final expression for the TRF kernel is

$$R_{\text{TRF}}(\tau,t) = -\mathrm{i}^3\langle\langle\boldsymbol{\mu}|\hat{\mathcal{G}}(\tau)\hat{\boldsymbol{\mu}}_R^l\hat{\mathcal{G}}(t)|\rho_{ee}^{(g)}\rangle\rangle \quad (20)$$

in calculation of Eq. (18) (we skipped $t_1 = 0$).

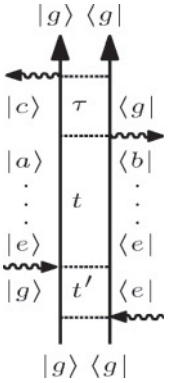

FIG. 3. Double-sided Feynman diagram corresponding to the time-resolved fluorescence.

This type of response function contribution to the TRF [Eq. (20)] is illustrated by the Feynman diagram presented in Fig. 3. The system starts in its ground-state population $|g\rangle\langle g|$. After two successive interactions (both happen within the single-laser excitation pulse), the excited-state population $|e\rangle\langle e|$ is created. The system then evolves in the excited state during the waiting time t (population transfer and population to coherence transfer events are possible), leaving the system in another state configuration $|a\rangle\langle b|$. Time τ separates two interactions after which the system returns to state $|g\rangle\langle g|$. The evolution during this last interval determines the emission spectrum, which is obtained by the Fourier transform.

Our assumptions describe the ideal experiment with maximum time and frequency resolution. On one side, we have vanishing interaction window, thus zero-time uncertainty, and on the other side, the perfect selectivity of excitons, i.e., zero-frequency uncertainty. This idealized case is never perfectly available. Realistic femtosecond pulses can not select specific excitons, while narrow-band pulses have picosecond time resolution. However, some systems have favorable setup of transition amplitudes that a specific exciton can be excited. For instance, only one exciton state carries most of the absorption intensity in J or H molecular aggregates.

The calculation of the fluorescence dynamics requires us to calculate the propagator $\hat{\mathcal{G}}(\tau)$ of the full density matrix, so all the information about the system and the bath is fully specified if the total density operator is known. That is easily accomplished for a single two-level system ($N = 1$) using the cumulant expansion,[29] which gives

$$R_{\mathrm{TRF}}(\tau,t) = \mathrm{i}^3 \exp[-\mathrm{i}(\varepsilon^0+\lambda)\tau]\exp\{-g^*(\tau) + 2\mathrm{i}\,\mathrm{Im}[g(t)-g(t+\tau)]\}, \tag{21}$$

where $g(t) = g'(t) + \mathrm{i}g''(t)$ is the lineshape function with its real and imaginary parts

$$g'(t) = \frac{\lambda}{\gamma}\cot\left(\frac{\beta\gamma}{2}\right)[\exp(-\gamma t)+\gamma t-1] + \frac{4\lambda\gamma}{\beta}\sum_{k=1}^{\infty}\frac{\exp(-\nu_k t)+\nu_k t-1}{\nu_k\left(\nu_k^2-\gamma^2\right)}, \tag{22}$$

$$g''(t) = -\frac{\lambda}{\gamma}[\exp(-\gamma t)+\gamma t-1]. \tag{23}$$

The sum in Eq. (22) is over the Matsubara frequencies $\nu_k = 2\pi k\beta^{-1}$. These equations were used to calculate the TRF of a single two-level system shown in Fig. 1.

The calculation of TRF for an aggregate if we go beyond the adiabatic approximation can not be given in terms of the lineshape functions. Instead, we solve equations of motion for the reduced density operator (RDO) of the system $\hat{\rho} = \mathrm{Tr}_{\mathrm{ph}}(\hat{\rho}_T)$ based on the hierarchical equations of motion.

C. HQME

Hierarchical equations of motion (HEOM) follow from the nonperturbative theory describing the exciton dynamics in the open quantum systems.[47] Because the usage of full theory is computationally expensive, here we utilize a modified HEOM theory termed by the authors as hierarchical quantum master equation (HQME).[45] It is still nonperturbational, but is restricted to the following approximate form of the bath correlation function:

$$\mathcal{C}_n(t) = \left(\frac{2\lambda_n}{\beta} - \frac{\beta\lambda_n\gamma_n^2}{6}\right)e^{-\gamma_n t} - \mathrm{i}\lambda_n\gamma_n e^{-\gamma_n t} + \frac{\lambda_n\gamma_n\beta}{3}\delta(t). \tag{24}$$

This form follows from Eq. (9) using the spectral density of Eq. (12) and expanding the Bose-Einstein function up to the $(\beta\omega)^1$ term (this expansion corresponds to [0/0] Padé decomposition of the spectrum[48]):

$$\frac{1}{1-e^{-\beta\omega}} = \frac{1}{\beta\omega} + \frac{1}{2} + \frac{\beta\omega}{12} + \mathcal{O}[(\beta\omega)^3]. \tag{25}$$

Conventional high-temperature approximation (HTA) schemes use only the first two terms of this expansion. Here, all three terms are used and the rest of the correlation function is accounted as the Markovian-white-noise residue ansatz.[45] In Fig. 4(a), we plot the real part of the bath correlation function obtained from Eq. (9) versus the exponential form in Eq. (24), which shows that the two functions are different only at short times (<10 fs). This part is additionally compensated by a delta-function term in Eq. (24).

The criterion of applicability certainly depends on temperature: it was shown to represent adequate dynamics when[45]

$$\zeta = \min\{\Gamma_n(\gamma_n)/\Omega_S, \kappa_n\} \gtrsim 2. \tag{26}$$

Here, $\Gamma_n(\gamma_n) = [\sqrt{12+(\beta\gamma_n)^2}+6]/\beta$, Ω_S is the characteristic frequency of the system and $\kappa_n = \sqrt{6\Gamma_n(\gamma_n)/(\beta\lambda_n\gamma_n)}$. We choose Ω_S to be equal to the exciton bandwidth.

The HQME for the correlation function given in Eq. (24) is written in the Liouville space as a hierarchy of coupled differential equations for auxiliary density operators (ADOs) denoted by $|\rho_{\mathbf{n}}(t)\rangle\rangle$ (Ref. 45):

$$\frac{d}{dt}|\rho_{\mathbf{n}}(t)\rangle\rangle = -\mathrm{i}\hat{\mathcal{L}}_e|\rho_{\mathbf{n}}(t)\rangle\rangle - \sum_{m=1}^{N}(\gamma_m n_m + \delta\hat{\mathcal{R}}_m)|\rho_{\mathbf{n}}(t)\rangle\rangle + \sum_{m=1}^{N} n_m\hat{\mathcal{A}}_m\left|\rho_{\mathbf{n}_m^-}(t)\right\rangle\rangle + \mathrm{i}\sum_{m=1}^{N}\hat{\mathcal{Q}}_m^{\times}\left|\rho_{\mathbf{n}_m^+}(t)\right\rangle\rangle, \tag{27}$$

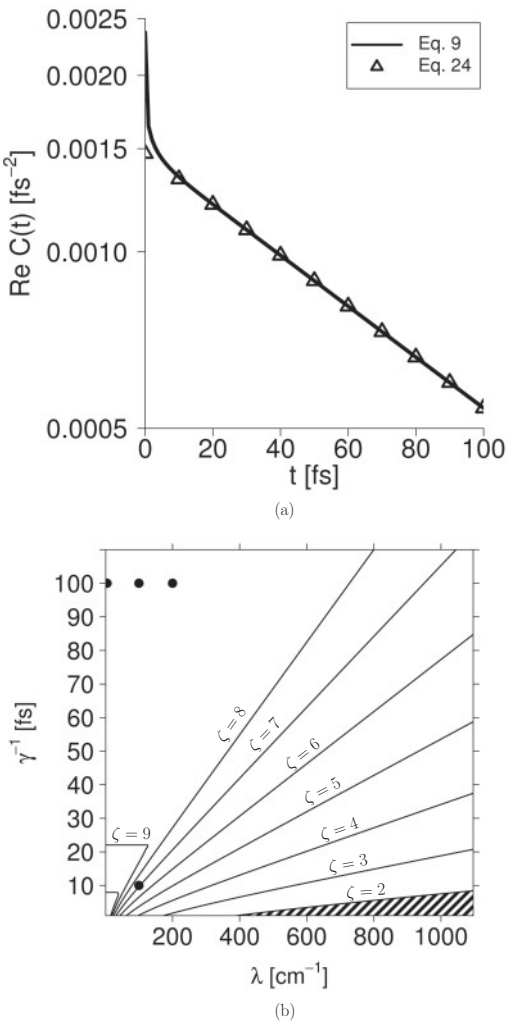

FIG. 4. (a) Real part of the bath correlation function for $T = 300$ K, $\lambda = 100$ cm^{-1}, $\gamma^{-1} = 100$ fs: full line is obtained by using Eq. (9) with the spectral density defined by Eq. (12) and the open triangles correspond to the exponential part of the expression given in Eq. (24). (b) 2D contour plot of ζ determining the HQME applicability when $T = 300$ K and $\Omega_S = 223.6$ cm^{-1} [see Eq. (26)]. Suitable space of parameters is confined by inequality $\zeta > 2$, while the space that is not suitable for HQME ($\zeta < 2$) is shaded. Points on the plot correspond to sets of parameters used in our simulations of the TRF spectra.

where the auxiliary superoperators

$$\delta\hat{\mathcal{R}}_m = \frac{\lambda_m\gamma_m\beta}{3}\hat{\mathcal{Q}}_m^{\times}\hat{\mathcal{Q}}_m^{\times}, \tag{28}$$

$$\hat{\mathcal{A}}_m = \mathrm{i}\left[\left(\frac{2\lambda_m}{\beta} - \frac{\beta\lambda_m\gamma_m^2}{6}\right)\hat{\mathcal{Q}}_m^{\times} - \mathrm{i}\lambda_m\gamma_m\hat{\mathcal{Q}}_m^{\circ}\right] \tag{29}$$

are introduced. Here, $\hat{\mathcal{Q}}_m^{\times}\bullet \Leftrightarrow [\hat{Q}_m,\bullet]$ ($\bullet$ is an arbitrary operator) denotes the commutator and $\hat{\mathcal{Q}}_m^{\circ}\bullet \Leftrightarrow \{\hat{Q}_m,\bullet\}$ is the anticommutator. In Eq. (27), $|\rho_{\mathbf{0}}(t)\rangle\rangle$ corresponds to the physical reduced density operator (RDO), $\mathbf{n}$ is a vector of indices $\mathbf{n} \equiv (n_1,n_2,\ldots,n_N)$, and we use notation $\mathbf{n}_m^{\pm} \equiv (n_1,n_2,\ldots,n_m \pm 1,\ldots,n_N)$. All ADOs with any negative index are set to zero.

Formally, the hierarchy in Eq. (27) is infinite, thus, the equations are nonperturbative and non-Markovian. In this paper, we adopt the simplest truncation scheme where all ADOs with their tier level $L = \sum_{m=1}^{N} n_m$ greater than truncation level L_{trunc} are simply discarded. Other truncation schemes are also possible.[42,49] The truncation level L_{trunc} was chosen to guarantee the convergence of the simulation results.

The HQME is used in the TRF as follows. The HQME propagates all ADOs; therefore, instead of Eq. (20) in accord with ADOs, we can define the hierarchy of response functions

$$R_{\mathbf{n}}^{\mathrm{TRF}}(\tau,t) = -\mathrm{i}^3\langle\langle\boldsymbol{\mu}|\hat{\mathcal{G}}_{\mathrm{ADO}}(\tau)\hat{\boldsymbol{\mu}}_R^l\hat{\mathcal{G}}_{\mathrm{ADO}}(t)|\rho_{\mathbf{n}}(t=0)\rangle\rangle, \tag{30}$$

where $\hat{\mathcal{G}}_{\mathrm{ADO}}(t)$ is the full propagator of the HQME and $R_{\mathbf{0}}^{\mathrm{TRF}}(\tau,t) \equiv R_{\mathrm{TRF}}(\tau,t)$ is the physically observable response function.[50] We calculate all propagations numerically by integrating ADO equations of motion using the standard fourth-order Runge-Kutta technique as implemented in the MATLAB software. The initial condition for simulation $|\rho_{\mathbf{n}}(t=0)\rangle\rangle$ assumes that the electronic state is e, while the bath is in the ground-state equilibrium, so $|\rho_{\mathbf{n}}(t=0)\rangle\rangle = \delta_{\mathbf{n},\mathbf{0}}|\rho_{ee}\rangle\rangle$ (nonzero ADOs correspond to system-environment correlations,[50] which are absent in the electronic ground state according to our Hamiltonian). Starting from this state, we then perform full HQME propagation for time t. After this propagation, we multiply all resulting ADOs $|\rho_{\mathbf{n}}(t)\rangle\rangle$ with the $\hat{\boldsymbol{\mu}}_R^l$. Next, propagation is for time τ and then we multiply resulting ADOs by $\langle\langle\boldsymbol{\mu}|$ to get $R_{\mathbf{n}}^{\mathrm{TRF}}(\tau,t)$. The relevant observable is given by only $R_{\mathbf{0}}^{\mathrm{TRF}}(\tau,t)$ (we can therefore ignore all nonrelevant ADOs during the last multiplication by $\langle\langle\boldsymbol{\mu}|$).

III. SIMULATIONS OF TIME-RESOLVED FLUORESCENCE SPECTRA OF AN EXCITONIC DIMER

In this section, we study the TRF spectra of the simplest molecular aggregate, a dimer constructed by a pair of coupled molecules. We thus have $N = 2$ and only two excited states $|1\rangle$ and $|2\rangle$ and the ground state $|g\rangle$. As mentioned earlier, the ground state is isolated. The exciton eigenstates of the electronic Hamiltonian of a dimer are labeled by $|e_1\rangle$ and $|e_2\rangle$.[1] Their wave functions make the transformation matrix between site basis and exciton basis, which can be given by the matrix

$$\hat{U} = \begin{pmatrix} \cos\theta & -\sin\theta \\ \sin\theta & \cos\theta \end{pmatrix}, \tag{31}$$

where

$$\theta = \frac{1}{2}\arctan\left(\frac{2J}{(\varepsilon_1^0+\lambda_1)-(\varepsilon_2^0+\lambda_2)}\right) \tag{32}$$

is the mixing angle ($-\pi/2 < \theta < \pi/2$). When the bath is neglected, the eigenstates are directly triggered by optical fields; they do not "see" chromophores, but see the eigenstates of the whole aggregate. The eigenstates are thus the main characteristic of the system. In the following discussion, we label excitonic states with increasing eigenenergy, so $\varepsilon_{e_1} < \varepsilon_{e_2}$.

In simulations, we use the dimer parameters resembling realistic molecular aggregates of dyes or photosynthetic complexes, where transition energies are in the visible range, e.g.,

20 000 cm^{-1} for the green light at 500 nm. This absolute shift is not relevant for exciton dynamics and can be neglected. We thus choose $\varepsilon_1^0 = 200$ cm^{-1}, $\varepsilon_2^0 = 100$ cm^{-1} for some weak asymmetry. The intermolecular coupling in various molecular aggregates ranges from 50 cm^{-1} in plant photosystem II (PS-II) and FMO to 500 cm^{-1} in bacterial circular aggregates or self-organized molecular J aggregates.[51] The important quantity, however, is the ratio of various energy parameters. We take the intermolecular coupling $|J| = 100$ cm^{-1} and the temperature is $T = 300$ K. The excitation and emission amplitudes are determined by the transition dipoles. For simplicity, we choose the transition dipoles of the dimer molecules to be parallel so that orientational averaging is not relevant. We choose molecular dipole moments to represent either H- or J-type aggregate by specifically setting transition dipole amplitudes. In the case of the H-type aggregate, we have $J > 0$ and we set molecular dipole moments to guarantee that transition to the lower-energy excitonic eigenstate is forbidden, $|\boldsymbol{\mu}_{e_1 g}| = 0$, (dark) and the other, higher-energy state is bright. The molecular dipole moments in this case are $\boldsymbol{\mu}_{1g} = (1, 0, 0)$ and $\boldsymbol{\mu}_{2g} = (\tan(\theta), 0, 0)$. In the case of the J-type aggregate, we have $J < 0$ and we set molecular dipole moments so that transition to higher-energy excitonic state is forbidden, $|\boldsymbol{\mu}_{e_2 g}| = 0$, and the transition to the lower-energy state is allowed. The molecular dipole moments in this case are $\boldsymbol{\mu}_{1g} = (1, 0, 0)$ and $\boldsymbol{\mu}_{2g} = (-\frac{1}{\tan(\theta)}, 0, 0)$ [note that since $J < 0$ and $\tan(\theta) < 0$, molecular dipole moments are collinear]. For simplicity, we also set $\lambda_1 = \lambda_2 = \lambda$ and $\gamma_1 = \gamma_2 = \gamma$, which is commonly justified for the same type molecules in the same environment. We will analyze how bath parameters λ and γ affect the TRF spectrum of the system under consideration.

At this point, we can check the applicability of HQME according to Eq. (26). In Fig. 4(b), we show a two-dimensional plot of the criterion [Eq. (26)] using $T = 300$ K and $\Omega_S = 223.6$ cm^{-1}, which for our dimer is the energy gap between the exciton states. All sets of parameters used in our TRF simulations, shown as points on the plot, appear in the range of validity.

To analyze how the TRF depends on the bath relaxation time γ^{-1}, we calculate TRF spectra of the H- and J-type aggregates by setting the system-bath coupling at $\lambda = |J| = 100$ cm^{-1}, which corresponds to the intermediate coupling regime. Figure 5 demonstrates the emission spectrum at various delay times for the H aggregate when the initial excitation at $t = 0$ is at $|e_2\rangle$. In all spectra, the emission maximum at initial times coincides with the corresponding single-exciton transition energy. When $\gamma^{-1} = 10$ fs, the Lorentzian lineshapes are observed in Fig. 5(a). This means that these parameters correspond to the Markovian or fast-bath dynamics regime. As γt goes from 0 to 1, the spectra remains unchanged, while at $\gamma t = 10$, we see a loss of the intensity that can be attributed to population transfer to the dark state. When $\gamma^{-1} = 100$ fs [Fig. 5(b)], the spectra evolves with the delay time much more dramatically. First, the lineshapes are Gaussian instead of Lorentzian as was the case for $\gamma^{-1} = 10$ fs. Second, the Stokes shift develops when γt goes from 0 to 1. Third, similar to the case of $\gamma^{-1} = 10$ fs, the e_2 peak loses intensity due to population escape at longer delay time; however, additionally, another lower-energy peak appears. In Fig. 6, we present the same type of the analysis for the J-type aggregate. The

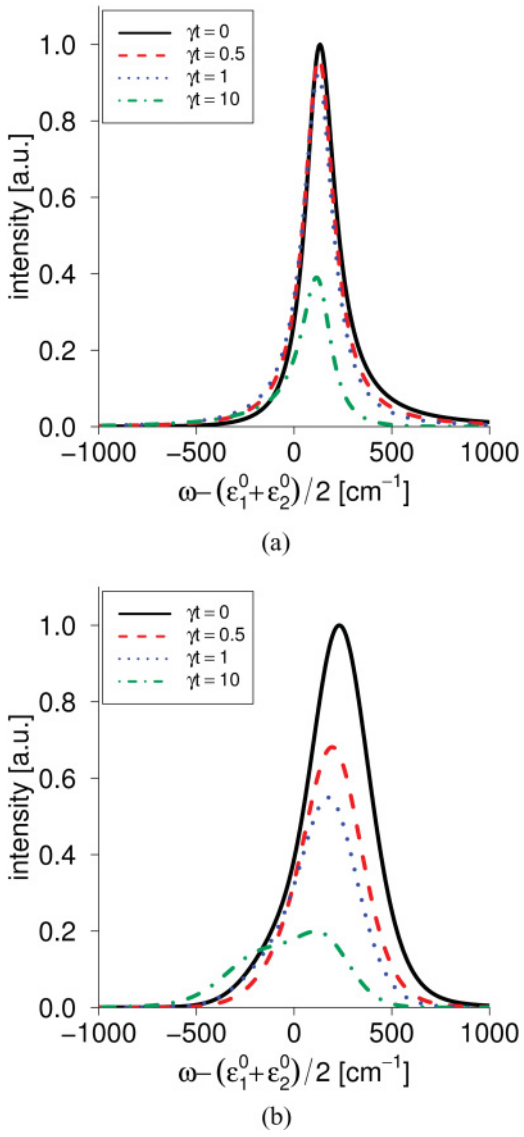

FIG. 5. (Color online) Time-resolved fluorescence spectra of the H-type dimer when (a) $\gamma^{-1} = 10$ fs, (b) $\gamma^{-1} = 100$ fs. λ is set to 100 cm^{-1}. All spectra here and in the following figures are normalized in such a way that, when delay time t is zero, the maximum intensity is equal to unity.

excitation at $t = 0$ appears at excitonic eigenstate $|e_1\rangle$ in this case. In Fig. 6(a), we see the Lorentzian lineshapes, clearly indicating that these parameters are in the Markovian regime. The peak intensity decreases with increasing the delay time. This can be attributed to population transfer to the second excitonic state. The other state is dark since it is not visible in the spectrum. When γ^{-1} increases to 100 fs, the lineshapes turn into Gaussian [see Fig. 6(b)] and the Stokes shift formation can be resolved very clearly. Further increase of γ^{-1} does not lead to any noticeable changes in the TRF spectra of either J- nor H-type aggregate when time is measured as γt (not shown).

What this simple analysis tells us is that fast-bath (Markovian) and slow-bath regimes lead to very different TRF spectra. The fast-bath case is in agreement with the Markovian exciton theory derived by using the Redfield approach: the

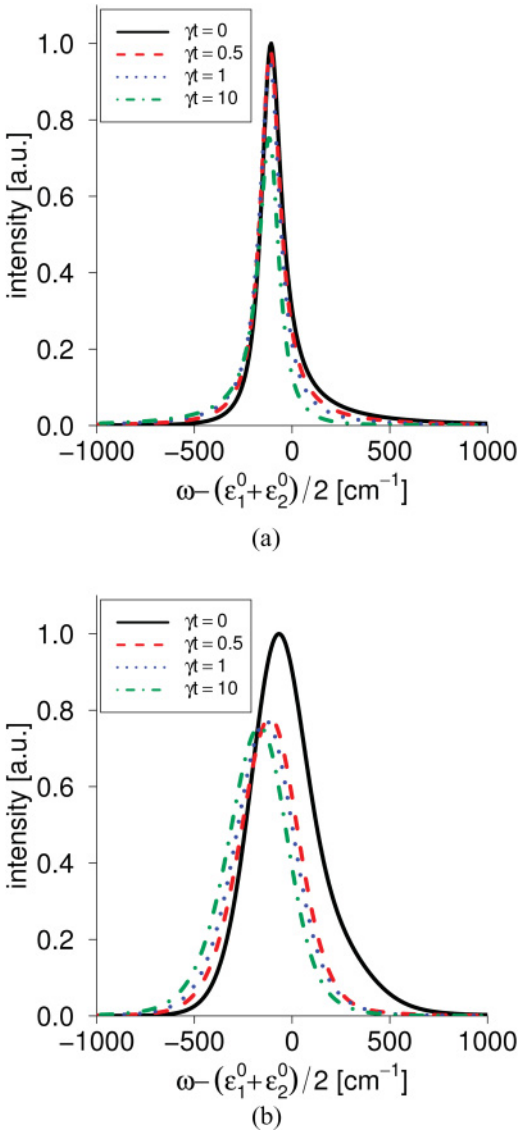

FIG. 6. (Color online) Time-resolved fluorescence spectra of the J-type dimer when (a) $\gamma^{-1} = 10$ fs, (b) $\gamma^{-1} = 100$ fs. λ is set to 100 cm^{-1}.

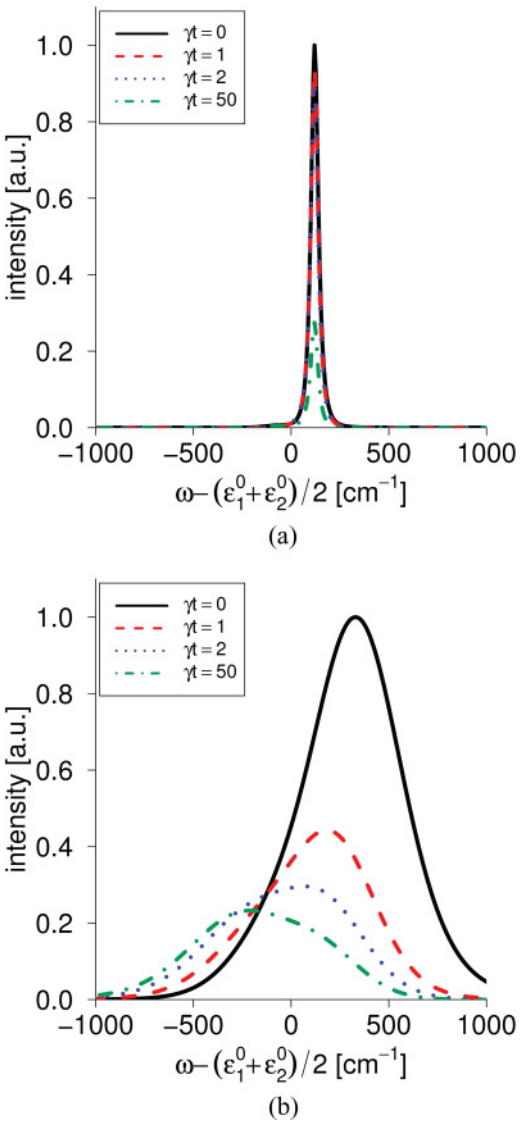

FIG. 7. (Color online) Time-resolved fluorescence spectra of the H-type dimer when (a) $\lambda = 5$ cm^{-1} and (b) $\lambda = 200$ cm^{-1}. γ^{-1} is set to 100 fs.

peak positions coincide with the exciton eigenstates, the peak lineshapes are Lorentzian, and the dark states defined according to the exciton representation are not visible in the spectrum. The slow bath creates much more complicated TRF dynamics: some effects, such as Gaussian lineshapes, emergence of the lower-energy peak in the H aggregate can not be explained in terms of the Markovian approach.

Next, we examine the effects of reorganization energy λ on the TRF spectra at $\gamma^{-1} = 100$ fs (we expect richer dynamics with this time scale according to the previous paragraph). Time-resolved spectra of the H-type dimer with different λ values are presented in Fig. 7. Again, the bright (second) excitonic eigenstate $|e_2\rangle$ was excited at $t = 0$. In the case of small reorganization energy [Fig. 7(a)], the spectral linewidth is narrow, the lineshape is Lorentzian, and the Stokes shift is absent. With the delay time, the emission peak drops due to population transfer. Thus, by reducing λ from 100 to 5 cm^{-1}, we recover the Markovian regime even at $\gamma^{-1} = 100$ fs. As expected, the increase of the reorganization energy to $\lambda = 200$ cm^{-1} [Fig. 7(b)] leads to wider peaks in the spectra. Also, the lineshapes change to Gaussian and the Stokes shift becomes clearly visible. In both cases, the intensity of the spectra decreases when delay time increases. However, in the case of bigger λ, we see again that the peak corresponding to the lower-energy state, which is dark in the exciton picture, emerges. The TRF spectra of the J-type dimer with different λ values, excited into the lower-energy bright state e_1 behaves similarly as follows from Fig. 8. In the case of small reorganization energy [Fig. 8(a)], the dynamics reflects the Markovian case, while when λ increases [Fig. 8(b)], the Stokes shift emerges. Also, we note that with the increase of delay time γt, the spectra loses some intensity due to population transfer to the dark higher-energy state. This is because while there is some upward population transfer, at thermal equilibrium the population of the lower energy state is much higher.

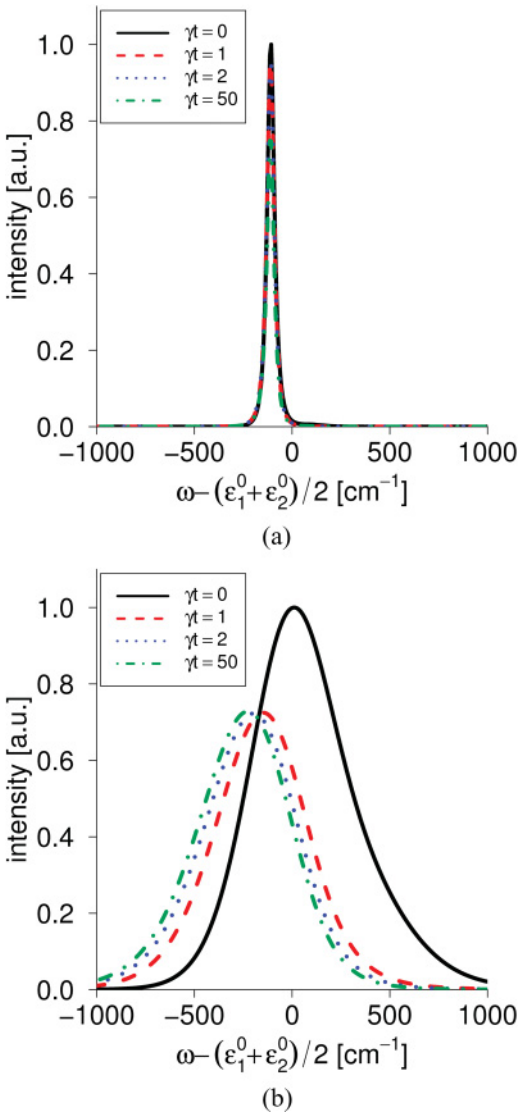

FIG. 8. (Color online) Time-resolved fluorescence spectra of the J-type dimer when (a) $\lambda = 5$ cm^{-1} and (b) $\lambda = 200$ cm^{-1}. γ^{-1} is set to 100 fs.

IV. SYSTEM DENSITY MATRIX DYNAMICS

The simulation results presented in the preceding section show that the TRF spectrum of a simple molecular aggregate strongly depends on the bath parameters λ and γ. Different dynamic regimes can be observed and several types of dynamical processes can be associated with the spectral dynamics. We can clearly distinguish two processes: the first is the bath relaxation after the excitation, the second is the system dynamics between different electronic levels due to the coupling with the bath.

In a single two-level molecule, the electronic dynamics is absent and only bath relaxation is taking place (see Fig. 1). It is noteworthy to mention that the analysis based on the cumulant expansion technique is equivalent to nonperturbative treatment of system-bath interaction via the HEOM theory. In the Markovian regime, the bath relaxation is faster than the signal formation, i.e., the relaxation time of the fluctuation correlation function is shorter than the induced polarization relaxation time. In that case, the optical measurements show the relaxed bath effects such as constant dephasing resulting in the Lotentzian lineshapes and absence of the Stokes shift. In the slow-bath regime, the bath does not relax before the emission event. We therefore can observe the bath relaxation, e.g., the dynamic Stokes shift, in the TRF measurements.

Parameter γ controls the TRF spectrum of a dimer as is the case of the monomer. For both H and J aggregates, when γ^{-1} is small [Figs. 5(a) and 6(a)], we find the Lorentzian lineshapes and no Stokes shift. Because the relaxation time scale of the bath correlation is very fast, the system reacts very quickly to external perturbations and thus the Stokes shift is absent. Note that not only the bath time scale is important for the Markovian regime, but also the system-bath coupling strength λ: the Markovian regime can be reached even with larger time γ^{-1} if the λ value is smaller. The Markovian regime for the dimer can therefore be described by the same inequality as is known for a monomer: $2\lambda k_B T \gamma^{-2} < 1$ denotes the Markovian regime and $2\lambda k_B T \gamma^{-2} > 1$ corresponds to the non-Markovian regime. The absence of the electronic relaxation (no population transfer) in the monomer is the only difference between the dimer and that of the monomer in the Markovian case. In the case of the J-type aggregate, the intensity of the emission spectra decreases only slightly since population is transferred to the higher exciton state. In the opposite, the emission decays considerably for the H aggregate since the population transfer is downward. Thus, in the Markovian regime, both J- and H-type aggregates behave along with the excitonic picture and the dynamics can be described by the Redfield theory.

When the bath time scale is intermediate or slow, the TRF dynamical properties of the molecular dimer are much more complicated. In this case, the dynamic Stokes shift emerges and it is significant similar to the case of the monomer. Results presented in Figs. 5(b) and 6(b) show that the time scale of the Stokes shift is clearly determined by γ. That is obviously the case in the monomer [see Fig. 1(c)]. In all cases, the shift is nearly complete when $\gamma t = 1$. That is related to the bath relaxation and it constitutes the dynamics in the case of a single molecule. However, the molecular dimer shows additional effects related to the excitation dynamics in the electronic subsystem. The most noteworthy result shown in Figs. 5(b) and 7(b) is the emergence of the lower-energy peak corresponding to the optically forbidden state in the case of the H-type aggregate. The same effect is also present in the J aggregate, however, it is weak since the population largely remains in the lowest, optically allowed state. Note that this effect contradicts the exciton picture, which states that amplitudes of the exciton transition are defined by the excitonic transition dipole moments and the zero transition should not be visible in the spectra. When $\lambda = 200$ cm^{-1}, this effect is strong, while it is weak when λ is only 5 cm^{-1} [see Fig. 7(b)]. The same can be seen in Fig. 5(b). The breakdown of the exciton picture is thus related to the value of reorganization energy and the time scale of the bath relaxation, i.e., it correlates with the breakdown of the Markovian regime. Thus, the non-Markovian system-bath regime destroys excitonic picture and the meaning of exciton eigenstates in the course of time.

In order to learn underlying system dynamics in these results, we simulated the evolution of the reduced density matrix of the system. In Fig. 9, we present evolutions of populations

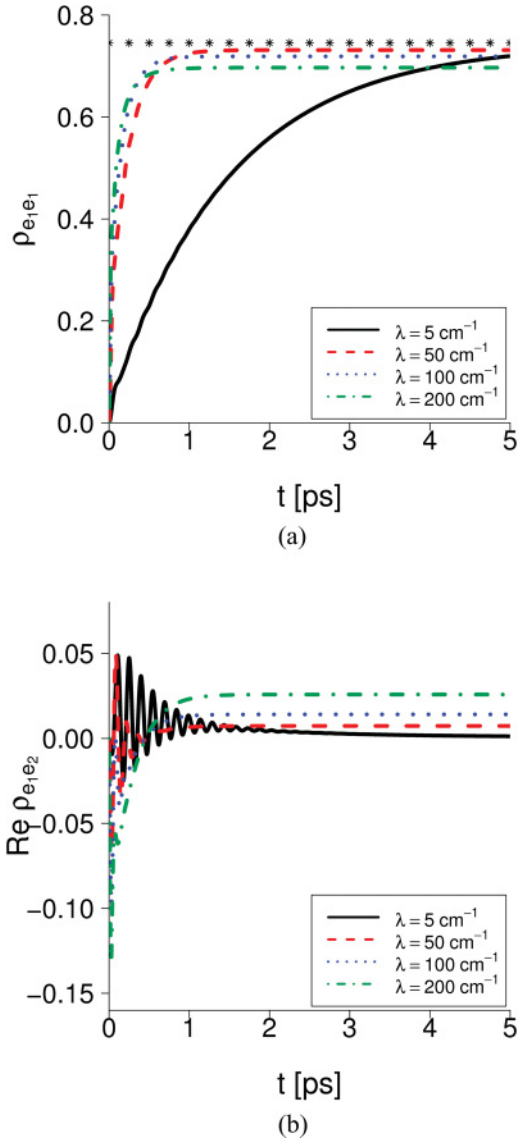

FIG. 9. (Color online) The evolution of the population of the lower-energy excitonic state (a) and coherence between excitonic states (b) of the H-type dimer (for parameters see text). Initial condition of propagation was $\hat{\rho}(0) = |e_2\rangle\langle e_2|$. The asterisk line in (a) corresponds to population of the first excitonic state according to the Boltzmann distribution.

and coherences involved in the TRF at different reorganization energies using the HQME theory. We have chosen the same parameters that were used in spectra calculations of Fig. 7(b), namely, $\varepsilon_1^0 = 200\ \text{cm}^{-1}$, $\varepsilon_2^0 = 100\ \text{cm}^{-1}$, $|J| = 100\,\text{cm}^{-1}$, $T = 300$ K, and $\gamma^{-1} = 100$ fs. Initial conditions were chosen as follows: $\hat{\rho}(0) = |e_2\rangle\langle e_2|$, once again corresponding to the case of the H dimer [see Fig. 7(b)]. The population of the first exciton state [see Fig. 9(a)] goes to equilibrium in about 2 ps except when the reorganization energy is small, $\lambda = 5\ \text{cm}^{-1}$. The obtained equilibrium should be comparable to the Boltzmann distribution between populations of the exciton eigenstates if the exciton description holds. However, the equilibrium populations do not match the Boltzmann distribution, as the value of $\rho_{e_1e_1}$ is lower than expected. This deviation is confirmed by inspecting excitonic coherences, which are expected to decay to zero. Evolutions of the excitonic coherences [Fig. 9(b)] show that, after initial oscillations, they reach constant equilibrium values depending on the reorganization energy. The fact that they do not decay to zero supports the conclusion that the distribution between the exciton states does not correspond to the Boltzmann equilibrium in this case.

This effect strongly depends on λ: equilibrium population values are closer to 0.5 than expected from the Boltzmann distribution with increasing λ. It means that effectively the energy gap between the true eigenstates, which take into account the bath, becomes smaller with increasing λ. All this indicates that the exciton eigenstates, which are obtained by diagonalizing the system part of the Hamiltonian, are no longer eigenstates of the combined system + bath supersystem. This behavior is similar to the polaron problem, where the increase of the system-bath coupling also effectively reduces the energy gap.[24]

The HEOM as the nonperturbative theory allows us to calculate the TRF independent of the chosen basis set. Moreover, the density matrix itself can be also represented in an arbitrary basis set. It is worthwhile to point out that the exciton basis (EB) as well as the site basis (SB) are not the true eigenstate basis of the whole system under consideration, including its environment. As follows from our analysis of the TRF, this eigenstate basis could also evolve in the course of time as the bath equilibrates. The asymptotic values of the reduced eigenstate basis for the whole system (the bath is traced out) can be obtained from the equilibrium conditions of the reduced density matrix. We denote this basis as the *global basis* (GB). The density matrix in the site basis can be transformed to the representation of the exciton eigenstates as

$$\hat{\rho}_{\text{EB}} = \hat{U}^{\dagger}\hat{\rho}_{\text{SB}}\hat{U} \tag{33}$$

by means of the unitary transformation given by Eq. (31). The transformation to the global basis can be similarly defined by

$$\hat{\rho}_{\text{GB}} = \hat{V}^{\dagger}\hat{\rho}_{\text{SB}}\hat{V}, \tag{34}$$

where $\hat{V}$ is an unknown unitary operator. Therefore, we need to find $\hat{V}$ in order to use the basis of the global eigenstates. It is known from the statistical physics that the ensemble-averaged equilibrium density operator must be diagonal in the GB representation. Thus, if we diagonalize the equilibrium density operator, we transfer it to its global eigenbasis

$$\hat{\rho}_{\text{GB}}^{\text{eq}} = \hat{V}^{\dagger}\hat{\rho}_{\text{SB}}^{\text{eq}}\hat{V}, \tag{35}$$

where $\hat{\rho}_{\text{GB}}^{\text{eq}}$ is diagonal. Since we calculate $\hat{\rho}_{\text{SB}}^{\text{eq}}$ by propagating the HQME, we can find $\hat{\rho}_{\text{GB}}^{\text{eq}}$ and $\hat{V}$ using the numerical diagonalization.

The knowledge of the relationship between the site and global basis allows us to investigate the effects of the bath on the electronic subsystem. As seen in Fig. 9(a), the increase of the reorganization energy effectively lowers the effective electronic energy gap in the system. The diagonal values of $\hat{\rho}_{\text{GB}}^{\text{eq}}$ correspond to equilibrium populations, from which we can recalculate the electronic energy gap of the GB basis:

$$\Delta_{\text{GB}} = \frac{1}{\beta}\ln\left(\frac{\left(\rho_{\text{GB}}^{\text{eq}}\right)_{\alpha_1\alpha_1}}{\left(\rho_{\text{GB}}^{\text{eq}}\right)_{\alpha_2\alpha_2}}\right), \tag{36}$$

where α_1 (α_2) denotes the lower- (higher-) energy eigenstate. So, Δ_{GB} is the energy gap between the global system eigenstates. Thus, the effective system Hamiltonian in the global eigenstate basis reads as

$$(\hat{H}_e)_{GB} = \begin{pmatrix} H_{\alpha_1\alpha_1} & 0 \\ 0 & H_{\alpha_1\alpha_1} + \Delta_{GB} \end{pmatrix}. \quad (37)$$

It is the Hamiltonian that governs the system equilibrium excited state, thus, it includes all bath-induced reorganization. Its elements should therefore depend on bath parameters γ, λ, and $k_B T$.

This procedure of finding the GB basis set requires explicit propagation of the excited state until the system reaches equilibrium. It shows dynamic flow of the basis-set functions, however, it is a numerically expensive procedure. When the intermediate steps of the relaxation are not important, e.g., in long-time steady state, it would be useful to derive how the bath asymptotically affects the original molecular Hamiltonian. In the following, we describe the possibility of the original Hamiltonian rescaling in order to directly obtain the equilibrated excited state.

Since we know the transformation operator $\hat{V}$, we can represent the Hamiltonian of Eq. (37) in the site basis by applying a unitary transformation

$$(\hat{H}_e)_{SB} = \hat{V}(\hat{H}_e)_{GB}\hat{V}^\dagger \equiv \begin{pmatrix} \varepsilon_1^{\text{eff}} & J_{\text{eff}} \\ J_{\text{eff}} & \varepsilon_2^{\text{eff}} \end{pmatrix}, \quad (38)$$

and we get the effective molecular Hamiltonian dressed up by coupling to the bath. This Hamiltonian represents the asymptotic effect of the bath, thus, one would "observe" this Hamiltonian in, e.g., stationary emission spectrum. We get two effective parameters: the effective energy gap between molecular states $\Delta_{SB}^{\text{eff}} = \varepsilon_2^{\text{eff}} - \varepsilon_1^{\text{eff}}$ and the effective coupling J_{eff}.

We have investigated how parameters Δ_{SB}^{eff} and J_{eff} depend on reorganization energy λ. These results are shown in Fig. 10. First, we note that since the excitonic picture is not perturbed in the case $\lambda \to 0$, the parameters corresponding to the effective Hamiltonian coincide with the parameters of the original Hamiltonian at small reorganization energy values. Second, the effect of λ to Δ_{SB}^{eff} is small, which means that the bath affects both molecules independently, the optical energy gaps of both molecules may change similarly, and the intermolecular energy gap Δ_{SB}^{eff} remains almost unaffected. To confirm this statement, it is worthwhile to mention that small dependence at large λ values is due to the HQME approach, while it disappears when using calculations based on the full HEOM theory. Third, effective coupling J_{eff} decreases strongly with increasing the reorganization energy, i.e., the molecules become more individual as the coupling to the bath increases. Therefore, it is an important parameter to describe the effects of the bath on the system.

We have additionally analyzed how J_{eff} depends on other parameters. Our results show that J_{eff} does not depend on molecular energies or γ, while it strongly depends on temperature. From our simulations, we find that in the case where the molecular reorganization energies λ_1 and λ_2 are different, the effective coupling can be accurately described by the following formula:

$$J_{\text{eff}} = J \exp\left(- a \frac{\lambda_1 + \lambda_2}{k_B T} \right), \quad (39)$$

where a is a constant (see Fig. 11). The numerical value of constant a was found to be 0.15. It can be seen that the exponential law gives an accurate estimate over a large range of $(\lambda_1 + \lambda_2)/(k_B T)$ values.

The fact that the effective coupling was found to increase with increasing temperature is opposite to predictions of the Holstein polaron theory.[24] In the Holstein Hamiltonian, each site is coupled to a single harmonic oscillator, which renormalizes stationary exciton (and the oscillator) states.[24,36] In our model, each site is coupled to a continuum of frequencies, and the system and whole bath relaxes to thermal equilibrium. Thus, our model considers the integral effect of the continuum surrounding. Formally, such perturbation is taken into account via the auxiliary density matrix elements

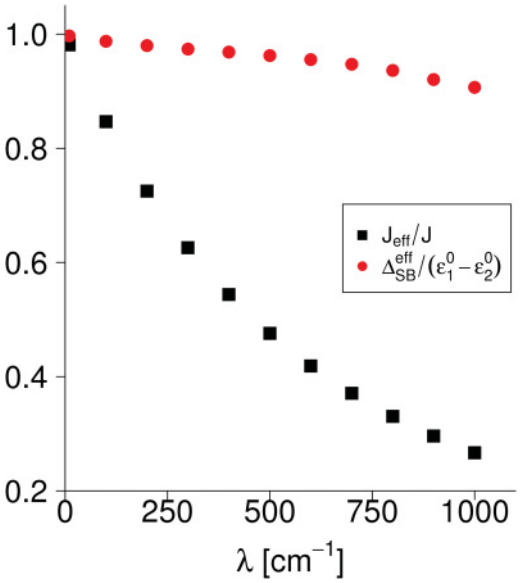

FIG. 10. (Color online) Dependence of effective system parameters on the reorganization energy.

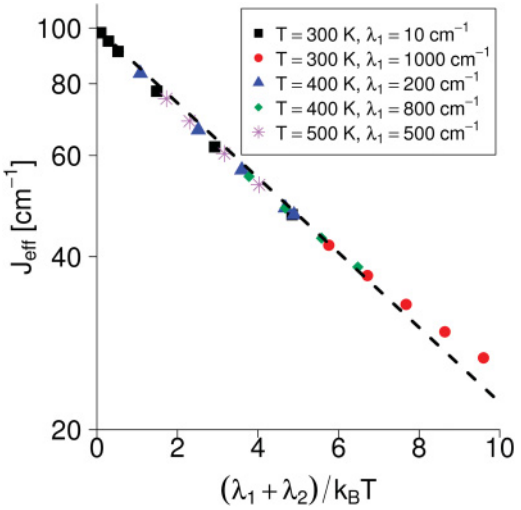

FIG. 11. (Color online) Effective coupling dependence on $(\lambda_1 + \lambda_2)/k_B T$. Black dashed line corresponds to values calculated by means of Eq. (39).

of the HQME. These differences are responsible for the differences in renormalization factor of the resonance coupling value.

Note, however, that our renormalization is for the relaxed electronic excited state. Only the emission properties depend on J_{eff}. The absorption spectrum reflects the relaxed ground electronic state, which reflects the J coupling. In order to find the J_{eff}, we have to perform a computationally expensive numerical propagation. However, we find an exponential renormalization relation with the bath parameters. The GB basis can now be achieved by inserting the effective couplings into the original Hamiltonian. In this way, we may need no numerical propagation. All we have to do is to diagonalize the system Hamiltonian, having replaced coupling J with effective coupling J_{eff}, which is defined by Eq. (39). We find exponential relation for an electronic dimer: it has to be proven that some similar relation can be derived for an arbitrary molecular aggregate. Obtaining the renormalized Hamiltonian parameters for an arbitrary system is our future research direction.

The exponential renormalization relation may be related to the properties of the spectral density. Our model of the bath has been used in a range of simulations. However, other spectral densities have been used in other simulations.[52,53] Realistic (determined from the spectral line-narrowing experiment) spectral density for pigment-protein aggregates is a multipeak function,[54] which can only be approximated by simple analytical functions. The sharp peaks in the spectral density are indications of high-frequency molecular vibrations strongly coupled to electronic transitions. These are important in some aggregates (e.g., some self-organized J aggregates[51]), however, they can be neglected for bacteriochlorophylls in FMO aggregate. We did not consider high-frequency coherent vibrational modes. The spectral density can be alternatively extracted by performing atomistic molecular-mechanics (MM) simulations,[55] which at the moment are a standard procedure for proteins, but have difficulties for interaction potentials describing the chlorophyll-based pigments. The HEOM can be written for an arbitrary spectral density,[40,50] however, its numerical implementation at the moment is possible only for simple bath models.

Our results clearly show that bare excitonic states might not be suitable to analyze the system in the case of strong-system bath coupling. Interaction with bath modes perturbs the system so that the coupling J is quenched and thus the energy difference between the eigenstates becomes lower. The introduction of effective bath coupling allows us to easily explain the emergence of the peak corresponding to lower-energy state in the TRF spectra of the H-type aggregate in Figs. 5(b) and 7(b). Reduction of the effective intermolecular coupling with system-bath coupling strength means that the excitons tend to shrink due to coupling to the bath, i.e., the exciton delocalization is smaller than predicted from bare excitonic couplings. The monomer dipole moments were chosen keeping the mixing angle definition of Eq. (32) in mind, and when $J \to J_{\text{eff}}$, this definition no longer guarantees that the dipole moment of the lower-energy state is zero.

Our renormalization is not static property. It develops dynamically in the electronic excited state. When the system is in the ground state, the exciton picture is not perturbed (no coupling to the bath). This has to be understood as the reference state and the excitons, which are created by the absorption event, are reference states. After excitation, the exciton basis starts to evolve due to system-bath coupling and the new effective excitons, which are more localized, develop in time. That picture may be very important for considering recent time-resolved experiments with femtosecond time resolution,[4,5,7] where such time-dependent exciton transformation could be traced out.

In our simulations, we did not consider the disorder effect on the system dynamics. Diagonal disorder creates inhomogeneous broadening. The inhomogeneous broadening can be approximated by static bath modes included into the spectral lineshape functions.[10] This induces Gaussian broadening, but excludes effects such as exciton localization. However, if the error of such protocol can be ignored, the resulting convolution procedure is numerically much faster than explicit statistical averaging over the disorder. The explicit simulation of the diagonal disorder exactly incorporates the static fluctuation effects. If we can distinguish fast and static modes of the bath, then the Redfield theory can be used for fast-bath modes: the static modes can be included explicitly by ensemble averaging.[9,12] That may be the most efficient strategy for large aggregates. However, our results demonstrate the dynamic bath effects such as dynamic formation of the Stokes shift, slow-bath-induced population transfer, which go beyond the static disorder. If these effects are important, then the HEOM theory should provide a more accurate solution.

V. CONCLUSIONS

We have studied exciton dynamics in a simplest molecular aggregate and found that the Markovian parameter regime guarantees accurate system dynamics within the excitonic eigenstate picture. The main signatures of the Markovian regime are the Lorentzian lineshapes and the conservation of excitonic symmetries imposed by molecular geometry. In the case of moderate and strong system-bath interaction, the excitonic picture becomes approximate and the system parameters have to be rescaled due to coupling with the bath similar to the polaron formation in molecular electronics. Then, the excitonic picture of the eigenstates becomes distorted, and the dark states may turn out in the spectrum.

The TRF spectroscopy is very powerful in displaying the details of the exciton relaxation and renormalization properties. Note that the absorption reflects the ground-state equilibrium configuration, and if the excitonic picture is based on that configuration (as is the case in the absorption), it may not be valid for the electronic excited state where the bath relaxes to a new minimum. The TRF explicitly displays that relaxation process, and the effective new set of system parameters for the electronic excitons of the excited bath equilibrium can be obtained.

Our theory of the TRF is derived for an arbitrary excitonic molecular aggregate with an arbitrary coupling strength to the bath. We did simulations only for a dimer. However, the important concepts of renormalization of the intermolecular couplings in the case of strong system-bath interaction in the electronic excited state is a general concept for an arbitrary aggregate. These renormalized parameters enter into the

energy-transfer rates, which dictate the functionality of the photosynthetic complexes and their efficiency. The quenching of the intermolecular coupling by the bath is important for J-type aggregates. It is known that for the aggregates having one molecule per unit cell, the exciton bandwidth equals to $4J$ in the case of nearest-neighbor couplings.[56] If J were quenched, it should be perceptible in the spectroscopy measurements (TRF or 2D spectra) as the peak position of the J band should be dependent on bath parameters.

Our results suggest a few promising areas that are worth further exploration. First, the full HEOM theory might be used to enlarge the range over which our effective coupling dependence on bath parameters hold, and when, if ever, it fails. Second, the effects of quenched coupling should be analyzed in the case of larger aggregates. Finally, it might be worthwhile to use the HEOM theory to study systems described by the Holstein Hamiltonian as polaron formation dynamics could be observed.

ACKNOWLEDGMENTS

The authors wish to thank V. Balevičius Jr. and V. Butkus for useful discussions. The present research was funded by the European Social Grant under the Global Grant measure. A.G. acknowledges support from a Student Research Fellowship from the Lithuanian Science Council.

*leonas.valkunas@ff.vu.lt

[1] H. van Amerogen, L. Valkunas, and R. van Grondelle, *Photosynthetic Excitons* (World Scientific, Singapore, 2000).
[2] T. Renger, V. May, and O. Kühn, Phys. Rep. **343**, 137 (2001).
[3] R. van Grondelle and V. I. Novoderezhkin, Phys. Chem. Chem. Phys. **8**, 793 (2006).
[4] G. S. Engel, T. R. Calhoun, E. L. Read, T. K. Ahn, T. Mančal, Y. C. Cheng, R. E. Blankenship, and G. R. Fleming, Nature (London) **446**, 782 (2007).
[5] H. Lee, Y.-C. Cheng, and G. R. Fleming, Science **316**, 1462 (2007).
[6] J. Kim, S. Mukamel, and G. D. Scholes, Acc. Chem. Res. **42**, 1375 (2009).
[7] G. S. Schlau-Cohen, A. Ishizaki, and G. R. Fleming, Chem. Phys. **386**, 1 (2011).
[8] D. Abramavicius, B. Palmieri, D. V. Voronine, F. Šanda, and S. Mukamel, Chem. Rev. **109**, 2350 (2009).
[9] I. Stiopkin, T. Brixner, M. Yang, and G. R. Fleming, J. Phys. Chem. B **110**, 20032 (2006).
[10] D. Abramavicius, L. Valkunas, and S. Mukamel, Europhys. Lett. **80**, 17005 (2007).
[11] V. Butkus, A. Gelzinis, and L. Valkunas, J. Phys. Chem. A **115**, 3876 (2011).
[12] D. Abramavicius and S. Mukamel, J. Phys. Chem. B **113**, 6097 (2009).
[13] P. Kjellberg, B. Brüggemann, and T. Pullerits, Phys. Rev. B **74**, 024303 (2006).
[14] D. Abramavicius, V. Butkus, J. Bujokas, and L. Valkunas, Chem. Phys. **372**, 22 (2010).
[15] T. Mančal, V. Balevičius, and L. Valkunas, J. Phys. Chem. A **115**, 3845 (2011).
[16] D. Emin and T. Holstein, Phys. Rev. Lett. **36**, 323 (1976).
[17] G. Wellein and H. Fehske, Phys. Rev. B **58**, 6208 (1998).
[18] P. E. Spencer, J. H. Samson, P. E. Kornilovitch, and A. S. Alexandrov, Phys. Rev. B **71**, 184310 (2005).
[19] A. Troisi, Phys. Rev. B **82**, 245202 (2010).
[20] H. Fehske, G. Wellein, and A. R. Bishop, Phys. Rev. B **83**, 075104 (2011).
[21] A. Damjanović, I. Kosztin, U. Kleinekathöfer, and K. Schulten, Phys. Rev. E **65**, 031919 (2002).
[22] G. Trinkunas and A. Freiberg, J. Lumin. **112**, 420 (2005).
[23] M. Pajusalu, M. Rätsep, G. Trinkunas, and A. Freiberg, ChemPhysChem **12**, 634 (2011).
[24] Y.-C. Cheng and R. J. Silbey, J. Chem. Phys. **128**, 114713 (2008).
[25] K. Hyeon-Deuk, Y. Tanimura, and M. Cho, J. Chem. Phys. **128**, 135102 (2008).
[26] T.-S. Ahn, A. M. Müller, R. O. Al-Kaysi, F. C. Spano, J. E. Norton, D. Beljonne, J.-L. Brédas, and C. J. Bardeen, J. Chem. Phys. **128**, 054505 (2008).
[27] A. V. Malyshev, V. A. Malyshev, and J. Knoester, Phys. Rev. Lett. **98**, 087401 (2007).
[28] R. Nakamura, N. Hamada, H. Ichida, F. Tokunaga, and Y. Kanematsu, J. Chem. Phys. **127**, 215102 (2007).
[29] S. Mukamel, *Principles of Nonlinear Optical Spectroscopy* (Oxford University Press, New York, 1995).
[30] V. May and O. Kühn, *Charge and Energy Transfer in Molecular Systems* (Wiley-VCH, Weinheim, 2004).
[31] M. Yang and G. R. Fleming, Chem. Phys. **275**, 355 (2002).
[32] T. Mančal, L. Valkunas, E. L. Read, G. S. Engel, T. R. Calhoun, and G. R. Fleming, Spectroscopy **22**, 199 (2008).
[33] A. Ishizaki and G. R. Fleming, J. Chem. Phys. **130**, 234110 (2009).
[34] Y.-C. Cheng and R. J. Silbey, J. Phys. Chem. B **109**, 21399 (2005).
[35] J. Olšina and T. Mančal, J. Mol. Model. **16**, 1765 (2010).
[36] T. Meier, Y. Zhao, V. Chernyak, and S. Mukamel, J. Chem. Phys. **107**, 3876 (1997).
[37] H.-P. Breuer and F. Petruccione, *The Theory of Open Quantum Systems* (Oxford University Press, New York, 2002).
[38] Y. Tanimura and R. Kubo, J. Phys. Soc. Jpn. **58**, 101 (1989).
[39] Y. Tanimura, Phys. Rev. A **41**, 6676 (1990).
[40] A. Ishizaki and G. R. Fleming, J. Chem. Phys. **130**, 234111 (2009).
[41] J. Strümpfer and K. Schulten, J. Chem. Phys. **131**, 225101 (2009).
[42] L. Chen, R. Zheng, Q. Shi, and Y. J. Yan, J. Chem. Phys. **131**, 094502 (2009).
[43] L. Chen, R. Zheng, Q. Shi, and Y. J. Yan, J. Chem. Phys. **132**, 024505 (2010).
[44] L. Chen, R. Zheng, Y. Jing, and Q. Shi, J. Chem. Phys. **134**, 194508 (2011).
[45] R. X. Xu, B. L. Tian, J. Xu, Q. Shi, and Y. J. Yan, J. Chem. Phys. **131**, 214111 (2009).
[46] B. L. Tian, J. J. Ding, R. X. Xu, and Y. J. Yan, J. Chem. Phys. **133**, 114112 (2010).
[47] Y. Tanimura, J. Phys. Soc. Jpn. **75**, 082001 (2006).
[48] J. Hu, M. Luo, F. Jiang, R. X. Xu, and Y. J. Yan, J. Chem. Phys. **134**, 244106 (2011).

[49]R. X. Xu, P. Cui, X. Q. Li, Y. Mo, and Y. J. Yan, J. Chem. Phys. **122**, 041103 (2005).
[50]K. B. Zhu, R. X. Xu, H. Y. Zhang, J. Hu, and Y. J. Yan, J. Phys. Chem. B **115**, 5678 (2011).
[51]T. Kobayashi, *J-aggregates* (World Scientific, Singapore, 1996).
[52]G. Raszweski, W. Saenger, and T. Renger, Biophys. J. **88**, 986 (2005).
[53]M. Cho, H. M. Vaswani, T. Brixner, J. Stenger, and G. R. Fleming, J. Phys. Chem. B **109**, 10542 (2005).
[54]V. I. Novoderezhkin, E. G. Andrizhiyevskaya, J. P. Dekker, and R. van Grondelle, Biophys. J. **89**, 1464 (2005).
[55]C. Olbrich, J. Strümpfer, K. Schulten, and U. Kleinekathoefer, J. Phys. Chem. Lett. **2**, 1771 (2011).
[56]H. Fidder, J. Knoester, and D. A. Wiersma, J. Chem. Phys. **95**, 7880 (1991).